Dynamics and efficiency of magnetic vortex circulation reversal

Michal Urbánek, Vojtěch Uhlíř, Charles-Henri Lambert, Jimmy J. Kan, Nasim Eibagi, Marek Vaňatka, Lukáš Flajšman, Radek Kalousek, Mi-Young Im, Peter Fischer, Tomáš Šikola, and Eric E. Fullerton

Phys. Rev. B **91**, 094415 — Published 16 March 2015

DOI: 10.1103/PhysRevB.91.094415

Dynamics and efficiency of magnetic vortex circulation reversal

Michal Urbánek,[1,2,*] Vojtěch Uhlíř,[1,3,†] Charles-Henri Lambert,[3] Jimmy J. Kan,[3] Nasim Eibagi,[3] Marek Vaňatka,[2] Lukáš Flajšman,[2] Radek Kalousek,[1,2] Mi-Young Im,[4,5] Peter Fischer,[4,6] Tomáš Šikola,[1,2] and Eric E. Fullerton[3]

[1] *CEITEC BUT, Brno University of Technology, Technická 10, 616 00 Brno, Czech Republic*
[2] *Institute of Physical Engineering, Brno University of Technology, Technická 2, 616 69 Brno, Czech Republic*
[3] *Center for Magnetic Recording Research, University of California, San Diego, 9500 Gilman Drive, La Jolla, California 92093-0401, USA*
[4] *Center for X-ray Optics, Lawrence Berkeley National Laboratory, 1 Cyclotron road, Berkeley, California 94720, USA*
[5] *Department of Emerging Materials Science, Daegu Gyeongbuk Institute of Science and Technology, Daegu 711-873, Korea*
[6] *Physics Department, University of California, 1156 High Street, Santa Cruz, California 94056, USA*

(Dated: February 17, 2015)

Dynamic switching of the vortex circulation in magnetic nanodisks by fast rising magnetic field pulse requires annihilation of the vortex core at the disk boundary and reforming a new vortex with the opposite sense of circulation. Here we study the influence of pulse parameters on the dynamics and efficiency of the vortex core annihilation in permalloy ($Ni_{80}Fe_{20}$) nanodisks. We use magnetic transmission soft x-ray microscopy to experimentally determine a pulse rise time – pulse amplitude phase diagram for vortex circulation switching and investigate the time-resolved evolution of magnetization in different regions of the phase diagram. The experimental phase diagram is compared with an analytical model based on Thiele's equation describing high amplitude vortex core motion in a parabolic potential. We find that the analytical model is in a good agreement with experimental data for a wide range of disk geometries. From the outputs of the analytical model and in accordance with our experimental finding we determine the geometrical condition for dynamic vortex core annihilation and pulse parameters needed for the most efficient and fastest circulation switching. The comparison of our experimental results with micromagnetic simulations show that the micromagnetic simulations of 'ideal' disks with diameters larger than ∼250 nm overestimate nonlinearities in susceptibility and eigenfrequency. This overestimation leads to the core polarity switching near the disk boundary, which then in disagreement with experimental findings prevents the core annihilation and circulation switching. We modify the micromagnetic simulations by introducing the 'boundary region' of reduced magnetization to simulate the experimentally determined susceptibility and in these modified micromagnetic simulations we are able to reproduce the experimentally observed dynamic vortex core annihilation and circulation switching.

PACS numbers: 75.75.Jn, 75.70.Kw, 85.75.-d, 68.37.Yz

I. INTRODUCTION

Magnetic vortices are curling magnetization structures formed in micro- and nanosized magnetic disks and polygons[1–5]. They are known for having four distinct magnetization configurations (vortex states) that can be used for a multibit memory cell[6,7]. The vortex states are defined by the polarity of the vortex core, pointing either up ($p = +1$) or down ($p = -1$) and by the circulation of the magnetization in the plane of the disk, curling either counterclockwise ($c = +1$), or clockwise ($c = -1$). The combination of the polarity and circulation defines the chirality (handedness) of the vortex. The vortex state can be controlled by applying a static out-of-plane (polarity control[8]) or in-plane (circulation control[9]) magnetic fields, although the amplitude of these fields can be quite large. However, both the polarity and the circulation can be switched more effectively by using fast-rising magnetic fields[10,11].

Selective switching of the circulation with applied magnetic field requires expelling the vortex core out of the disk and then reforming a new vortex with the opposite sense of spin circulation. We have recently demonstrated[11], that this can be achieved by using a fast rising in-plane magnetic field pulse that drives the vortex core into far-from-equilibrium gyrotropic precession and annihilates the vortex during the first half-period of the precessional motion at the disk boundary. The resulting circulation of a new vortex is controlled by a disk asymmetry in the form of a thickness gradient and by the direction of the magnetic field pulse. This approach allows for a fast switching with the field amplitudes reduced by more than 50% when compared to the switching using static fields.

The dynamics of a magnetic vortex confined in soft ferromagnetic nanodisks excited resonantly by an in-plane alternating magnetic field or by a fast rising magnetic field pulse can be described as a forced harmonic oscillator using Thiele's equation of motion[12,13]. The resulting magnetic response depends on the profile of the confining magnetostatic potential. The potential can be described either by parabolic terms[14,15], or more precisely including higher order terms in the energy expansion[16–18]. Micromagnetic simulations predict significant contribution of higher order energy terms[16,17] leading to a nonlinear increase of the eigenfrequency as a function of

the vortex core position. However, the experimental results obtained from eigenfrequency measurements at high-amplitude rf-field excitations or low amplitude rf-field excitations in a biasing field are often inconsistent with the simulations, showing a decrease of the eigenfrequency with an increasing amplitude[19] or a pinning dominated dependence on the eigenfrequency[20,21]. Only recently, an experimental measurement of anharmonicity of a potential well in a FeV single crystal disk showed a ∼10% increase of the eigenfrequency for vortex core displacements up to $0.4R$, where R is the radius of the disk[18].

In this paper, we present an experimental and modeling study of the process of dynamic annihilation of the magnetic vortices in micro- and nanosized magnetic disks. We investigate the range of disk diameters and thicknesses, in which the magnetic vortices can be dynamically annihilated, as well as possible extension of this range by an appropriate selection of the pulse rise time and amplitude. The experimental results are presented in section II. In section III we describe a simple, but well-fitting analytical model based on Thiele's equation of motion assuming a parabolic potential. In section IV we compare the experimental data and the analytical model with micromagnetic simulations. The discrepancy between the prediction of micromagnetic simulations and experimental data is discussed and a modified micromagnetic simulation, fitting to the experimental observations is presented.

II. EXPERIMENTS

The dynamic annihilation of magnetic vortices was studied on a series of samples consisting of permalloy ($Ni_{80}Fe_{20}$) disks with diameters ranging from 250 nm to 2500 nm and thicknesses from 20 nm to 50 nm. The disks were placed on gold coplanar waveguides which were used to generate in-plane magnetic field pulses up to 60 mT. To provide a circulation control, the disks were fabricated with a wedge-like thickness asymmetry using the shadowing effect of a 500-nm-thick polymethyl methacrylate (PMMA) mask and a directional ion beam sputtering of $Ni_{80}Fe_{20}$ with the sputtered particles incident at 15° from the film normal[11]. The entire structure was fabricated on a 200-nm-thick, 2×2 mm-wide Si_3N_4 membrane to allow for sufficient x-ray transmission in the magnetic transmission soft x-ray microscopy (MTXM)[22] experiments [Fig. 1(b)].

Magnetic field pulses were generated by launching current pulses into the waveguide using a pulse generator (Agilent 81150A) allowing a precise setting of the rise time in the range of 2.5–8.0 ns and the amplitude of the pulses in the range of 1.0–50.0 mT. The pulse shapes were recorded on a 4-GHz real-time oscilloscope (LeCroy WaveMaster 804Zi-A). Alternatively, for smaller disks where a faster rise time was needed, a fast pulse generator (Picosecond Pulse Labs 10,050A) with a fixed rise time of 250 ps was used.

The magnetization in the disks and its temporal behavior was imaged with full-field transmission soft x-ray microscope at beamline 6.1.2 at the Advanced Light Source (ALS) in Berkeley, CA. Images with a spatial resolution of 25 nm were recorded using x-ray magnetic circular dichroism (XMCD) as magnetic contrast for a fixed circular polarization of the x-ray beam at the Fe L_3 edge (707 eV). The sample normal was tilted at an angle of 30° with respect to the x-ray beam to measure the in-plane magnetization component. The disks were imaged before, during and after application of the magnetic field pulses. The time-resolved experiments, which recorded snapshots of magnetization in the disks at defined times during the magnetic pulse, were based on a pump-probe technique enabling stroboscopic imaging of reproducible events[23]. The temporal resolution is given by the length of the photon flashes (70 ps), which arrive in the two-bunch operational mode of the ALS at 3.05 MHz repetition frequency [Fig. 1(a)]. The total acquisition time for each image is about 120 s, i.e. approximately 3.7×10^8 events are averaged to obtain a single image [Fig. 1(c)].

Prior to the application of magnetic field pulses we set the spin circulation in a disk into one state (e.g. clock-

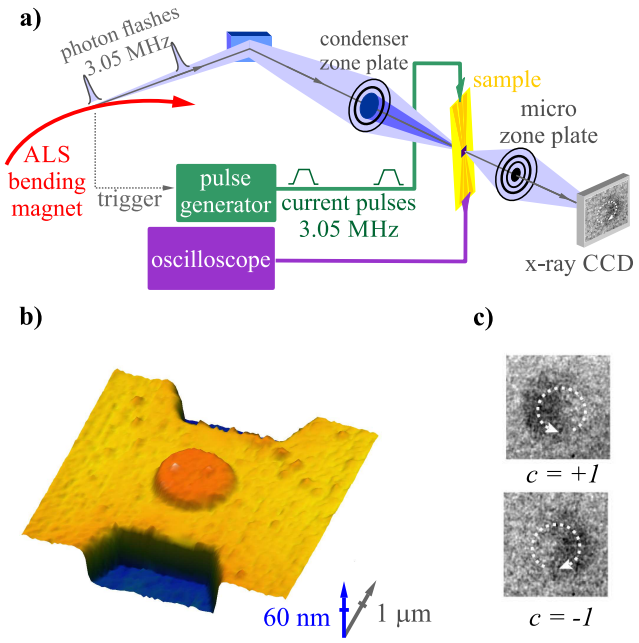

FIG. 1: (a) Experimental setup of time-resolved experiments. Photon flashes from the ALS were synchronized with current pulses from a pulse generator. Time-resolved images of the magnetization were recorded by varying the delay between the field pulses and the photon flashes. (b) Atomic Force Microscopy image of the sample consisting of 1600-nm-wide, 20-nm thick nanodisk on top of a 2500-nm-wide, 60-nm thick waveguide. A wedge-like thickness asymmetry is on the right side of the disk. (c) Magnetic contrast in the images of the nanodisk with counterclockwise ($c = +1$) and clockwise ($c = -1$) spin circulations.

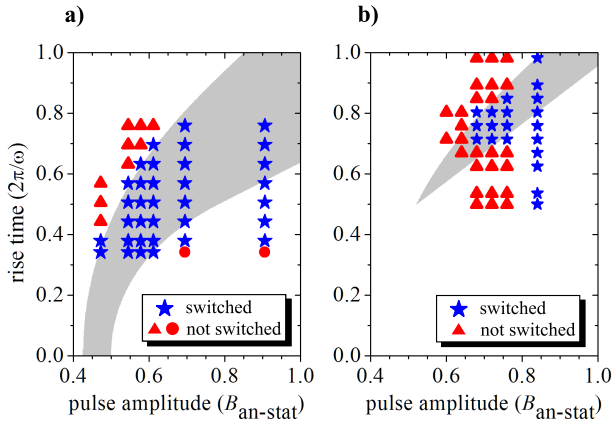

FIG. 2: (a) Pulse rise time—pulse amplitude phase diagram experimentally determined for a 1600-nm-wide, 20-nm-thick permalloy disk with an estimated eigenperiod $2\pi/\omega = 7.9$ ns and experimentally determined static annihilation field $B_{\text{an-stat}} = 19$ mT. The pulse rise times and pulse amplitudes are given in units of the gyrotropic oscillation period ($2\pi/\omega$) and vortex static annihilation field ($B_{\text{an-stat}}$), respectively. Red triangles represent a case of unsuccessful switching. Blue stars represent a case, where successful core annihilation led to a circulation switching. Red dots represent a case, where the circulation switching was not achieved in spite of using shorter rise time and larger pulse amplitudes. (b) Phase diagram for a 1600-nm-wide, 30-nm-thick permalloy disk. The region of successful circulation switching moved towards top-right of the normalized phase diagram. The grey areas in the phase diagrams define boundary of the region of successful circulation switching predicted by the analytical model (see section III).

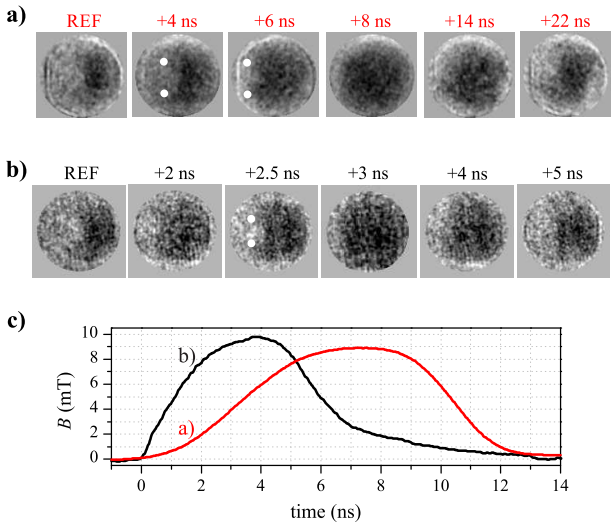

FIG. 3: (a)+(b) Temporal evolution of magnetization in a 1900-nm-wide and 20-nm-thick disk during magnetic field pulses captured by series of time-resolved MTXM images. (a) Temporal evolution of magnetization showing full saturation at 8 ns which is followed by nucleation of a new vortex at 14 ns. (b) represents a case where the vortex annihilation was not achieved in spite of using larger pulse amplitudes than in (a). Here, the maximum displacement of the vortex core was reached at 3 ns. At 4 ns the vortex core(s) return towards the disk center, indicating a continuous motion of the core without vortex annihilation and re-nucleation. Symmetric contrast in the MTXM images is a combination of two symmetric core trajectories and thus indicates the core polarity reversal (either at vortex nucleation after its annihilation or directly during the core motion). (c) Profiles of the pulses used in (a) and (b). The rise times of the pulse are 4 ns and 2.4 ns, respectively (measured between 10% and 90% of the pulse amplitude).

wise) by applying an external static magnetic field in a defined direction exploiting the asymmetry in the disk thickness[11]. The pulsed magnetic field was then applied in the opposite direction and in case of a successful annihilation of a vortex the spin circulation in the disk switched (i.e. from clockwise to counterclockwise and vice versa). In case of unsuccessful annihilation, the circulation stayed the same. These data allowed for construction of a pulse rise time—pulse amplitude phase diagram of successful vortex annihilation (see Fig. 2). It is possible to distinguish three distinct regions: (1) a region of low pulse amplitude and long rise time [Figs. 2(a), (b); red triangles], where a circulation switching was not observed, (2) a region of intermediate pulse amplitude and intermediate rise rime [Fig. 2(a), blue stars], where the circulation switching was detected and finally (3) a region of short rise time and high amplitude [Fig. 2(a), red dots], where again the circulation switching was not successful.

Time resolved experiments revealed the dynamics in each region. In region (1) the vortex core was not expelled out of the disk and gyrated freely in the disk with an unchanged polarity (data not shown). In region (2) the pulse parameters were sufficient to expel the vortex core out of the disk [see Fig. 3(a)]. After an intermediate state where the disk was fully saturated a new vortex with a defined circulation and a random polarity is formed[11]. The symmetric magnetic contrast apparent in these images corresponds to two vortex core trajectories for two opposite polarities of the vortex core[24], which were averaged together during a multitude of cycles of the pump-probe technique. When applying pulses with a shorter rise time the dynamics significantly changes [see Fig. 3(b)]. We observe the same symmetric contrast revealing core polarity switching, but the disk did not reach a full saturation in contrast to the situation in Fig. 3(a). Hence, the symmetric contrast cannot originate from random nucleation of the core polarity. This suggests that the core polarity flipping during the core motion prevented vortex annihilation and consequent circulation reversal, even when a stronger pulse than in region (2) was applied. Profiles of the two magnetic pulses are indicated in Fig. 3(c).

The described behavior was consistent over all disk geometries. The character and boundaries of the normalized diagram stayed the same for disks with the same thickness, even when the radius was changed. With in-

creasing disk thickness the region (2) shrank towards top-right of the normalized phase diagram [Fig. 2(b)]. In section III we present an analytical model describing the underlying processes in the phase diagram.

III. ANALYTICAL MODELING

A vortex core trajectory in a magnetic disk during dynamic annihilation can be described by an analytical model based on Thiele's equation of motion[12,25]. When using a fast rising magnetic pulse $\mathbf{B} = [0, B]$ with a rise time shorter or equal to the period of the vortex eigenoscillation, the vortex core $\mathbf{C} = [x, y]$ gyrates about a point $\mathbf{S} = [s, 0]$, following a circular trajectory. The distance of the gyration center from the disk center is $s = R\chi B/(\mu_0 M_s)$, where R is the disk radius, χ is the static susceptibility of the vortex, B is the applied magnetic field and M_s is the spontaneous magnetization of the disk material[26]. As the coordinates of the gyration center depend on the magnitude of the magnetic field B, during the rise time of the magnetic pulse the point $\mathbf{S}$ is moving perpendicularly to the direction of the magnetic field with a velocity $v_s = R\chi B_{max}/(\mu_0 M_s t_{rise})$, where B_{max} is the maximum amplitude of the pulse and t_{rise} is the rise time of the pulse. Hence, assuming a linear rise time, the resulting trajectory of the vortex core is cycloidal with coordinates: $x(t) = v_s[t - (1/\omega)\sin\omega t]$, $y(t) = (v_s/\omega)(1-\cos\omega t)$, where ω is the eigenfrequency of the gyrotropic mode. When the maximum amplitude of the pulse B_{max} is reached at $t = t_{rise}$, the vortex core trajectory changes to circular with a gyration center (static equilibrium point) at a distance $s_{max} = R\chi B_{max}/(\mu_0 M_s)$ from the disk center [see Fig. 4(a)]. For detailed description of the model see Appendix A.

The maximum amplitude of the vortex translational motion $x_{max} = s_{max} + |\mathbf{C}(t_{rise}) - \mathbf{S}_{max}|$ needs to fulfil the geometrical condition for the successful vortex annihilation: $x_{max}(B_{max}, t_{rise}) \geq R_{an}$, where R_{an} is the annihilation radius. The vortex core is annihilated, when its distance from the disk center reaches R_{an}, which is smaller than R due to the finite size of the vortex core. The value $R_{an} \sim 0.85R$ was estimated from experimental data fitting the upper boundary of the phase diagram [see Fig. 2(a) and Fig. 4(a), (b)] and confirmed by micromagnetic simulations [see section IV and Fig. 7(c)].

A second condition to be considered is associated with the vortex core velocity. If the core velocity exceeds the critical velocity[27,28] the core polarity is switched and the sense of the vortex core gyration is reversed[24]. The polarity reversal causes an offset of the initial core position before it continues gyrating about the point $\mathbf{S}$ and as a result, the maximum amplitude of the vortex core translational motion is reduced. Although the vortex core may still reach the annihilation radius after polarity switching, it is at the cost of a significantly increased pulse amplitude[35] and this case is not considered in the model. The experimental data confirming the reduced

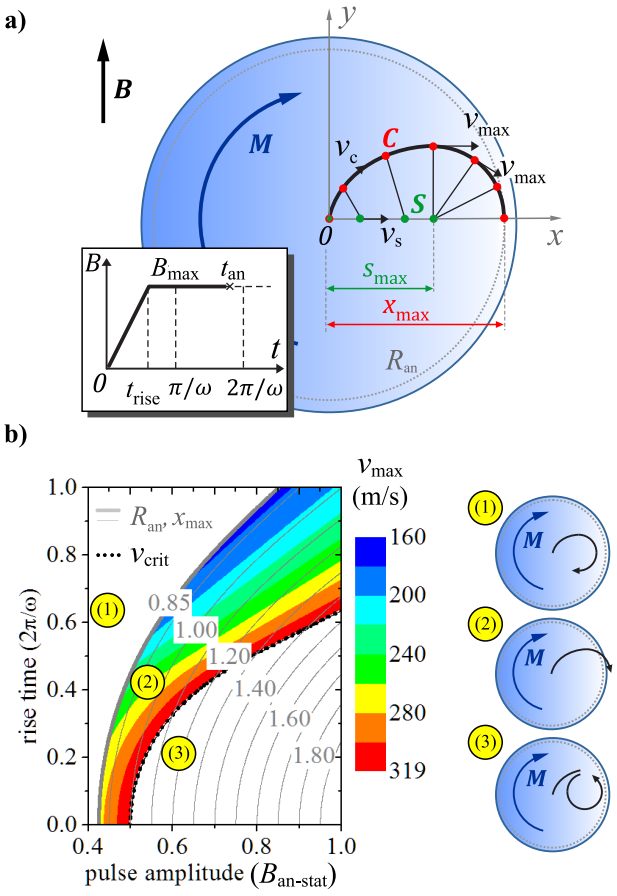

FIG. 4: (a) Sketch of the trajectory of the vortex core during a magnetic field pulse with a rise time. During the rise time of the magnetic pulse the gyration center $\mathbf{S}$ is moving perpendicularly to the direction of the magnetic field with a velocity v_s. The trajectory of the vortex core is cycloidal. At the maximum amplitude of the pulse B_{max} the vortex core trajectory changes to circular with a gyration center at a distance s_{max}. The vortex core is annihilated, when its maximum amplitude of the vortex translational motion x_{max} reaches the annihilation radius R_{an}. (b) Rise time – pulse amplitude phase diagram showing the region of successful vortex core annihilation [color-coded, marked (2)]. The pulse rise times, pulse amplitudes and maximum amplitudes of the vortex translational motion are given in units of the gyrotropic oscillation period ($2\pi/\omega$), vortex static annihilation field ($B_{an\text{-}stat}$) and the disk radius (R), respectively. The region is defined by the two boundaries; the annihilation radius R_{an} (thick gray line at $x_{max} = 0.85R$) and the critical velocity v_{crit} (black dotted line at $v_{cmax} = 320\,\mathrm{m\,s^{-1}}$). For the rise time – pulse amplitude combinations in the region [marked (1)] above the annihilation radius boundary, the maximum amplitude of the translation motion of the vortex core is too low and the core gyrates inside the disk. For the rise time – pulse amplitude combinations in the region (3) below the critical velocity boundary the core switches its polarity and reverses its sense of gyration. The phase diagram is calculated for 20-nm-thick permalloy disks with following material parameters: $M_s = 6.9\times10^5\,\mathrm{A\,m^{-1}}$, $\gamma = 2.9\times10^{11}\,\mathrm{rad\,Hz\,T^{-1}}$, $v_{crit} = 320\,\mathrm{m\,s^{-1}}$.

efficiency of the magnetic field pulse in the core-flipping regime can be found in Appendix B. For efficient dynamic switching (i.e. without core polarity reversal), the following condition for the maximum vortex core velocity $v_{\max}$ must be satisfied: $v_{\max}(B_{\max}, t_{\rm rise}) < v_{\rm crit}$, where $v_{\max} = ((2s_{\max})/t_{\rm rise})\sin((\omega t_{\rm rise})/2)$ for $t_{\rm rise} \leq \pi/\omega$ and $v_{\max} = ((2s_{\max})/t_{\rm rise})$ for $t_{\rm rise} \geq \pi/\omega$ (see Appendix A). For our model we use a value of $v_{\rm crit} = 320\,{\rm m\,s^{-1}}$[27], which corresponds to our experimental data[36].

These conditions set a limit on the amplitude and rise time of the magnetic pulse needed for successful and efficient vortex core annihilation and form boundaries in a phase diagram displaying the region of successful switching [color-coded area in Fig. 4(b)]. The region is marked by two boundaries. The first boundary results from the condition that the vortex core must reach the annihilation radius [thick gray line in Fig. 4(b)] and the second boundary is the result of the condition for the critical velocity [black dotted line in Fig. 3(b)].

Input parameters for the model are the rise time $t_{\rm rise}$, the pulse amplitude $B_{\max}$, the disk radius R, the thickness L, its susceptibility χ, and its eigenfrequency ω. The pulse parameters $t_{\rm rise}$ and $B_{\max}$ are used for the construction of a phase diagram displaying the region of successful vortex annihilation [Fig. 4(b)] for disks with a given geometry. The last two parameters in the model (χ and ω) can be either determined experimentally or calculated from the material parameters of the modeled disk. It has been shown, that the susceptibility can be predicted with reasonable precision by the rigid-core model[26] and the eigenfrequency by the pole-free model[25]. Since the eigenfrequency dependence on the disk geometry is proportional to L/R[25], the vortex core velocity during gyration is proportional to the disk thickness L only (from $\omega \propto L/R$ and $|\mathbf{C}-\mathbf{S}| \propto R$ it follows that $v_{\rm c} = \omega|\mathbf{C}-\mathbf{S}| \propto L$). We can also normalize the pulse rise time by the period of the eigenoscillation and pulse amplitude by the static annihilation field. As a result, the shape of the phase diagram is the same for all disk diameters and depends on the thickness only. The lowest amplitude boundary remains the same for all thicknesses in the normalized phase diagram [see Fig 4(a)]. The intersection of the lowest amplitude boundary with the pulse amplitude axis at zero rise time indicates the minimum pulse amplitude which is sufficient to annihilate the vortex [$\sim$0.43 of the static annihilation field for our permalloy disks, see Figs. 5(a), (b)]. The boundary for the critical velocity is moving to the top-left with increasing thickness [see Fig. 5(a)] and at a certain threshold [$\sim$23 nm for our permalloy disks, see Fig. 5(b)] it is no longer possible to annihilate the vortex with a pulse with a zero rise time. By increasing the rise time, it is still possible to dynamically annihilate the vortex in thicker disks at the cost of an increased pulse amplitude. Finally, for disks thicker than 36.9 nm the minimum pulse amplitude equals the static annihilation field $B_{\rm an-stat}$ [Fig. 5(b)].

The pulse parameters, the rise time $t_{\rm rise}$, the pulse amplitude $B_{\max}$ and the minimum pulse duration $t_{\rm an}$ (i.e.

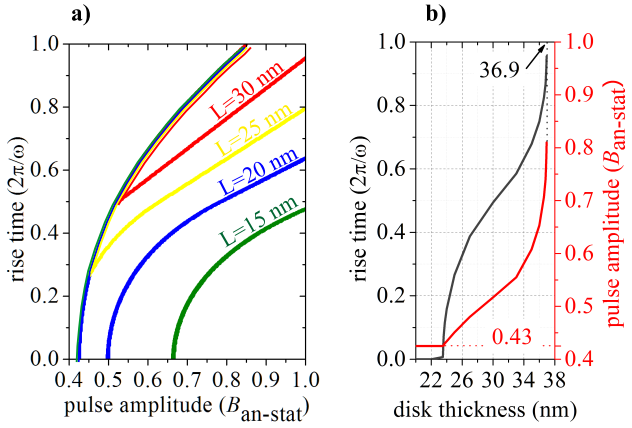

FIG. 5: (a) Phase diagram showing the regions of successful vortex core annihilation in permalloy disks with different thicknesses. The pulse rise times and pulse amplitudes are given in units of the gyrotropic oscillation period ($2\pi/\omega$) and vortex static annihilation field ($B_{\rm an\text{-}stat}$), respectively. The lowest amplitude boundary on the left remains the same for all thicknesses. The critical velocity boundary is moving to the top-left with increasing disk thickness, i.e. the region of successful core annihilation is progressively shrinking. (b) Thickness dependence of the minimum pulse amplitude (red line) and the corresponding minimum pulse rise time (black line) needed for successful vortex core annihilation. For the disks with a thickness of 23 nm or less, the minimum pulse amplitude is $0.43B_{\rm an-stat}$. For disks with thicknesses above 36.9 nm the model does not predict the possibility of dynamic annihilation of the core with a pulse amplitude lower than $B_{\rm an-stat}$ [the thickness limit is calculated assuming the same material parameters as in Fig 4(b)].

the predicted time at which the core reaches the annihilation radius $R_{\rm an}$) can be used to calculate the energy cost associated with the vortex annihilation (resp. the circulation switching). Mapping the energy cost for each point in the region (2) of the phase diagram allows to find the specific pulse parameters for which the vortex annihilation is most efficient. Since the exact pulse energy $E = \int_0^{t_{\rm an}} RI^2 dt$ (R is the electrical resistance of the waveguide and I is the electric current) depends on the resistance of the waveguide used to generate the magnetic field pulse, we calculate the reduced energy ε from the magnetic field pulse: $\varepsilon = \int_0^{t_{\rm an}} B^2 dt$. Assuming a linear rise time, we get $\varepsilon = B_{\max}^2(t_{\rm an} - \frac{2}{3}t_{\rm rise})$ for the case where $t_{\rm an} \geq t_{\rm rise}$ and $\varepsilon = \frac{1}{3}t_{\rm an}(B_{\max}t_{\rm an}/t_{\rm rise})^2$ when $t_{\rm an} \leq t_{\rm rise}$, i.e. the core is annihilated before the (theoretical) maximum pulse amplitude is reached. In Figs. 6(a)-(c) the reduced energy is plotted in the pulse rise time – pulse amplitude phase diagrams for the disks with thicknesses L of 15, 20 and 30 nm. For disks with thicknesses below $\sim$20 nm, the most effective switching occurs when the pulse amplitude is slightly above the minimum value ($B_{\max} = 0.47B_{\rm an-stat}$) and the rise time is short, but nonzero [$t_{\rm rise} = 0.17(2\pi/\omega)$]. The region is marked by hashes in Figs. 6(a)-(b). For thicker disks the phase dia-

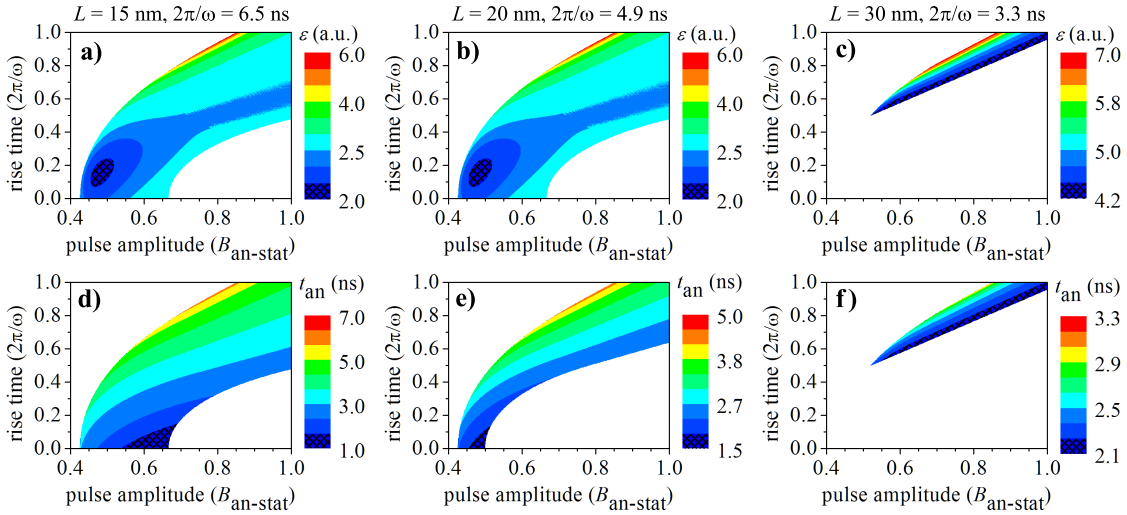

FIG. 6: Pulse rise time - pulse amplitude phase diagrams showing the reduced energy ε needed for the vortex circulation switching (a)-(c) and shortest annihilation times $t_{\rm an}$ (d)-(e). The pulse rise times and pulse amplitudes are given in units of the gyrotropic oscillation period ($2\pi/\omega$) and vortex static annihilation field ($B_{\rm an\text{-}stat}$), respectively. The regions of the most efficient switching (least energy cost) and shortest annihilation times are marked by hashes. The phase diagrams were calculated for permalloy disks with a radius $R = 500$ nm and thicknesses $L = 15$, 20 and 30 nm. Material parameters used for calculation of the phase diagrams were the same as in Fig. 4.

gram becomes restricted by the critical core velocity and successful vortex annihilation cannot be achieved with short rise times. Then, the region of the most effective switching is located along the bottom-right boundary of the phase diagram and starts already at the minimum pulse amplitude [Fig. 6(c)].

The regions of fastest switching [Figs. 6(d)-(f), marked by hashes] are located around the minimum rise time and maximum pulse amplitude, i.e. the right boundary of the phase diagram. By comparing the absolute values of ε in Figs. 6(a)-(c) and $t_{\rm an}$ in Figs. 6(d)-(f), we can see that the switching becomes more efficient with decreasing disk thickness and also the time to annihilation can be shortest in thinnest disks. However, for thinner disks the position of the region of the fastest switching does not correspond to the region of minimum ε [compare Fig. 6(d) and Fig. 6(a), respectively] and the choice between fast or efficient switching must be made.

Note, that the positions of the energy and pulse duration minima are independent of the disk radius and depend on the disk thickness only.

IV. MICROMAGNETIC SIMULATIONS

The predictions of the analytical model agreed with micromagnetic simulations[37] only for disks with radii R up to ∼125 nm. For larger disks and independent of thickness, the vortex core velocity exceeded the critical velocity within few picoseconds after the beginning of the pulse which lead to core polarity switching. Micromagnetic simulations predict large nonlinearity in the dimensionless displacement susceptibility $\chi_d = (ds/dB)(B_{\rm an\text{-}stat}/R)$ [Fig. 7(a); orange line with circles]. Due to this nonlinearity, at the beginning of the pulse where the displacement susceptibility is higher, the gyration center in micromagnetic simulation is located further out than the linear model predicts. For instance, a pulse amplitude $B = 0.5B_{\rm an\text{-}stat}$ corresponds to a gyration center $\mathbf{S}$ at $s = 0.5R$ according to the linear model [Fig. 7(a) grey line], whereas according to micromagnetic simulations the initial position of $\mathbf{S}$ is at $s = 0.85R$ [Fig. 7(a) orange line with circles]. This increase in the gyration radius leads to an increase of the core velocity above the critical velocity. We can overcome the unwanted polarity switching at the beginning of the pulse by using a pulse with a nonzero rise time.

However, when the core approaches the disk boundary, its velocity again exceeds the critical velocity, which leads to polarity reversal and a consequent change in the sense of gyration [see Fig. 7(b)]. This reversal at the disk boundary, which is always present in simulations of disks with radii larger than ∼500 nm is caused by an anharmonicity in the potential energy well, which for large vortex core displacements leads to an increase in eigenfrequency[16,17,29,30]. From the dimensionless displacement susceptibility $\chi_{\rm d}(s)$, we can obtain the local eigenfrequency $\omega(s) = \frac{\mu_0}{8\pi}\gamma M_{\rm s}\frac{\xi^2}{\chi_{\rm d}(s)}$, where we assume $\xi = 2/3$ (pole-free model magnetization distribution[25]). Note that this approach is more suited for the calculation of the eigenfrequency of small amplitude vortex core gyration about a gyration center position $\mathbf{S}$ shifted from the disk center by a static biasing field[20]. In our case of a large gyration amplitude, the eigenfrequency at the position $\mathbf{C}$ of the vortex core is lower[29]. The local eigenfre-

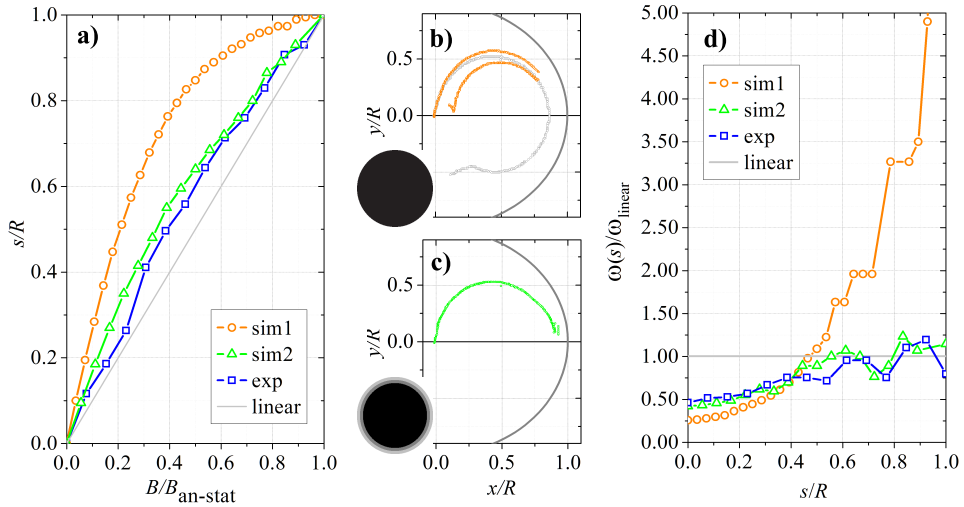

FIG. 7: (a) Comparison of simulated displacement susceptibility of the 1600 nm wide, 20 nm thick disk with uniform M_s (sim1 – orange line with circles), simulated displacement susceptibility of the same disk, where the spontaneous magnetization of the disk material was gradually decreased from 690 kAm^{-1} to 310 kAm^{-1} in the 80-nm-wide region around the disk perimeter (sim2 – green line with triangles) and the displacement susceptibility determined directly from the experimental measurements of the shift of the vortex core in an increasing applied magnetic field by MTXM (exp – blue line with squares). Linear susceptibility, used in analytical models is plotted as a gray line. (b) Simulated vortex core trajectories in the disk with uniform magnetization (nonlinear susceptibility). A magnetic field pulse of 10 mT is not enough to reach the annihilation radius (gray trajectory). A slight increase of the magnetic field amplitude to 11 mT drives the vortex core into the nonlinear region, where the eigenfrequency of the translational motion and thus also the vortex core velocity are increased, which leads to unwanted polarity switching. Switched core then continues with inverted sense of gyration towards the disk center (orange trajectory). (c) Simulated vortex core trajectory in the disk with magnetization decreasing towards the edge (linearized susceptibility). A magnetic pulse of 9 mT is sufficient to drive the vortex core into the annihilation region and the vortex is successfully annihilated (green trajectory). (d) Comparison of local eigenfrequencies $\omega(s)$ calculated from displacement susceptibilities in (a).

quency $\omega(s)$ rapidly increases for the core displacements larger than $0.6R$ [see Fig. 7(d) orange line with circles]. The increase in eigenfrequency drives the core velocity above the critical value and the core polarity close to the disk boundary switches [Fig. 7(b)].

This result of micromagnetic simulation is in contradiction to our experimental observations, where we were able to annihilate the vortex core in disks with radii up to 1.25 μm. To quantify the nonlinearity in displacement susceptibility we tracked the vortex core position as a function of static magnetic field. The spatial resolution of MTXM allowed us to directly measure a shift of the vortex core in an applied magnetic field with sub-100-nm precision. Comparison of the experimentally measured displacement susceptibility for 1600-nm-wide, 20-nm-thick disk [Fig. 7(a); blue line with squares] with micromagnetic simulation [Fig. 7(a); orange line with circles] reveals clearly the overestimation of the nonlinearity in displacement susceptibility by the micromagnetic simulation.

We were able to reproduce the experimental displacement susceptibility curve in micromagnetic simulations [see Fig. 7(a)], blue line with squares and green line with triangles, respectively) by gradual decrease of the spontaneous magnetization of the disk material near the edge [from 690 kA m^{-1} to 310 kA m^{-1} in the 80-nm-wide 'boundary zone', see insets in Figs. 7(b) and 7(c)]. By including this modification, it is possible to annihilate the vortex also in micromagnetic simulations [see Fig. 7(c)]. The eigenfrequency calculated from corrected simulation and from experimentally measured displacement susceptibility stays close to the eigenfrequency used in the linear model [see Fig. 7(d)] and the vortex core can reach the annihilation radius without exceeding the critical velocity.

The linear behavior of the displacement susceptibility in real disks may be caused by shape imperfections, lateral roughness and other deteriorations of the magnetic properties of the disk material close to the disk edge, e.g. by oxidation. It cannot be explained by the lateral roughness only, because the lateral roughness at the edges of our disks was approximately 20 nm (estimated from SEM images), whereas the width of the boundary region necessary for reproducing the experimental data is 4× larger. Also, it cannot be explained by the thickness gradient at one side of the disk as the susceptibility curve was measured on the side without the thickness asymmetry. We observed an additional increase of the nonlinearity in displacement susceptibility for larger disks, however the experimentally determined nonlinearity in displacement susceptibility was still significantly smaller than the predictions of micromagnetic simula-

tions (2.5-μm-wide disks, data not shown). Similar, weaker than expected nonlinearity in displacement susceptibility was reported for 3-μm-wide permalloy disks measured by Lorentz transmission electron microscopy by Uhlig et al.[31]. The existence of a higher-order term (beyond the parabolic approximation) in the potential energy well resulting in a parabolic dependence of eigenfrequency on the core displacement and 10% increase at $\sim 0.3R$ was recently reported in FeV single crystal disks[18]. In our case, a similar dependence in experimentally determined eigenfrequency can be seen for static core displacements up to $0.4R$ [Fig. 7(d)]. Beyond this point the experimental data do not follow a clear trend (i.e. parabolic dependence) and stay in the vicinity of ω_{linear}. This comparison shows that for large amplitude vortex core gyrations the assumption of linear susceptibility provides a good approximation and that the micromagnetic simulations of 'ideal' disks grossly overestimate the nonlinearity in displacement susceptibility (anharmonicity of the vortex potential well) for large core displacements.

V. CONCLUSIONS

We have studied the influence of the pulse parameters on the dynamics and efficiency of the vortex core annihilation in permalloy nanodisks. The experimentally determined pulse rise time – pulse amplitude phase diagram was successfully reproduced with an analytical model based on Thiele's equation describing vortex core motion in a parabolic potential. We found that the analytical model is in good agreement with experimental data for a wide range of disk geometries. From both the analytical model and the experimental findings we have determined the geometrical condition for dynamic vortex core annihilation and the pulse parameters giving the most efficient and fastest circulation switching. However, micromagnetic simulations of the vortex core annihilation in 'ideal' disks did not fully reproduce the experimental behavior. This is due to the fact that the nonlinearities in displacement susceptibility and eigenfrequency of 'ideal' disks with diameters larger than $\sim$250 nm are overestimated with respect to the experimentally determined values. This overestimation leads to a core polarity switching near the disk boundary which prevents the core annihilation and subsequent circulation switching. We modified the micromagnetic simulation by introducing a 'boundary region' of reduced magnetization to simulate the experimentally determined displacement susceptibility. This results in linearization of the displacement susceptibility and the modified micromagnetic simulation shows a good agreement of the dynamic vortex core annihilation with the experimental observations. Assumption of a nonparabolic potential with higher order energy terms, which may be more precise for the description of vortex core motion within $0.4R$ from the disk center[18], does not provide a significant correction to the parameters inferred from the linear susceptibility model. We conclude that the linear susceptibility model (i.e. a parabolic potential) is appropriate for the description of the first period of the high amplitude vortex core gyration in real disks.

Acknowledgments

The research at BUT was supported by the European Regional Development Fund (CEITEC – CZ.1.05/1.1.00/02.0068), by the Grant Agency of the Czech Republic (Project No. P102/12/P443) and the EU seventh Framework Programme (Contracts No. 286154–SYLICA and 280566–UnivSEM). The research at UCSD was supported by the research programs of the US Department of Energy (DOE), Office of Basic Energy Sciences (award #DE-SC0003678). The operation of the x-ray microscope was supported by the Director, Office of Science, Office of Basic Energy Sciences, Materials Sciences and Engineering Division, of the U.S. Department of Energy under Contract No. DE-AC02-05-CH11231. PF and MYI acknowledge support by the Leading Foreign Research Institute Recruitment Program (Grant No. 2012K1A4A3053565) through the National Research Foundation of Korea (NRF) funded by the Ministry of Education, Science and Technology (MEST).

Appendix A: Description of the analytical model

The relation between the position of the vortex core and the external static in-plane magnetic field in the disk made from soft-magnetic material can be described by the rigid vortex model[26]:

$$s = \frac{R\chi B}{\mu_0 M_{\text{s}}}, \tag{A1}$$

where s is the displacement of the vortex core from the disk center, R is the disk radius, χ is the vortex susceptibility depending on the geometrical parameters of the disk, B is the external magnetic field, and M_{s} is the spontaneous magnetization of the disk material. In the following calculations, the susceptibility χ is assumed to be independent of the core displacement. The equation of motion of the vortex core in time-varying external magnetic field can be described by Thiele's equation[12], which is derived from the Landau-Lifshitz-Gilbert equation of magnetization dynamics assuming the vortex core moves as a rigid object. Thiele's equation is as follows:

$$\mathbf{G} \times \dot{\mathbf{C}} - \frac{\partial W}{\partial \mathbf{C}} = \mathbf{F}(t), \tag{A2}$$

where $\mathbf{G} = -2\pi p L M_{\text{s}}/\gamma \hat{\mathbf{z}}$ is the gyrovector, $\mathbf{C}$ is the position of the vortex core, W is potential energy associated with the force restoring the vortex core back to the disk center, and $\mathbf{F}(t) = -\frac{2}{3}\pi c L R M_{\text{s}}(\mathbf{B}(t) \times \hat{\mathbf{z}})$ is the time-dependent excitation force associated with the applied

in-plane magnetic field[32]. The parameter p is the vortex core polarity, c is the circulation, L is the disk thickness, R radius and γ is the gyromagnetic ratio. The potential energy W is mainly defined by the magnetic dipolar energy[17] and can be approximated by a parabolic term

$$W = \frac{1}{2}\kappa \mathbf{C}^2, \tag{A3}$$

where κ can be understood as a stiffness constant. According to our experimental results higher order terms in the expression of potential energy need not to be taken into account as discussed in the paper.

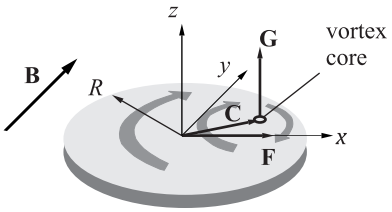

FIG. 8: Magnetic disk with a vortex magnetization ($p = -1$, $c = -1$). Position of the vortex core (open circle) is represented by vector $\mathbf{C} = (x, y, 0)$, the gyrovector by $\mathbf{G} = (0, 0, G) \propto -p\hat{\mathbf{z}}$. External force due to the applied in-plane magnetic field $\mathbf{B} = (0, B, 0)$ is described by vector $\mathbf{F} = (F, 0, 0) \propto -c(\mathbf{B} \times \hat{\mathbf{z}})$.

In the following calculations we choose the co-ordinate system in the following way: the origin coincides with the disk center and z axis is parallel with the disk axis of symmetry, the gyrovector points in the direction of $\hat{\mathbf{z}}$: $\mathbf{G} = (0, 0, G)$ and $\mathbf{C} = (x, y, 0)$, see Fig. 8.

If the applied magnetic field is zero, i.e. $\mathbf{F} = \mathbf{0}$, we obtain from (A2) the following homogeneous set of first-order ordinary differential equations:

$$\dot{y} + \frac{\kappa}{G}x = 0, \qquad \dot{x} - \frac{\kappa}{G}y = 0 \tag{A4}$$

which leads to a set of two separated second-order differential equations:

$$\ddot{x} + \left(\frac{\kappa}{G}\right)^2 x = 0, \qquad \ddot{y} + \left(\frac{\kappa}{G}\right)^2 y = 0. \tag{A5}$$

Solutions of both equations represent harmonic oscillations of both components with equal translational eigenfrequency $\omega \equiv \kappa/|G|$. According to the discussion on our experimental results, besides χ also ω can be considered as independent from the position of the vortex core. Therefore, the trajectory of the vortex core is a circle with a center located at the disk center and an arbitrary radius lower than R.

The solution of Thiele's equation (A2) with general time dependence of the external force $\mathbf{F}(t)$ needs to be calculated numerically. However, assuming a magnetic field pulse with a linear rise time (see Fig. 9), the motion of the vortex core can be treated analytically, as described in the next paragraph.

1. Analytical solution of Thiele's equation

We consider the initial state as following: At the beginning the vortex core is located at the disk center having zero velocity, i.e.

$$x(0) = y(0) = \dot{x}(0) = \dot{y}(0) = 0. \tag{A6}$$

Furthermore, without loss of generality, we will consider that the external force acts only in the direction of x axis, i.e. $\mathbf{F}(t) = [F(t), 0, 0]$, see Fig. 8. Then the set of first-order ordinary differential equations is according to (A2) as follows:

$$\dot{y} + \omega x = F(t)/G, \qquad \dot{x} - \omega y = 0 \tag{A7}$$

By solving these equations for a constant external force F_0 we obtain a circular vortex core trajectory with a center at $\mathbf{S} = (s, 0, 0)$ and a radius s, where $F_0 = \kappa s$.

If we consider a linear rise of the magnetic field from zero to a maximum value $B_{\max}$ during a time interval $\langle 0; t_{\mathrm{rise}}\rangle$ where $t_{\mathrm{rise}} \leq 2\pi/\omega$, the instantaneous position $\mathbf{S}$ is moving along the x-axis with a velocity

$$v_s = \frac{s_{\max}}{t_{\mathrm{rise}}}, \tag{A8}$$

where

$$s_{\max} = \frac{R\chi B_{\max}}{\mu_0 M_{\mathrm{s}}} \tag{A9}$$

is the x-position of $\mathbf{S}$ at the instant t_{rise}. The vortex core velocity can be obtained by solving the set of two equations (A7) with $F(t) = \kappa v_s t$, i.e.

$$\ddot{x} + \omega^2 x = \omega^2 v_s t, \qquad \ddot{y} + \omega^2 y = \omega v_s. \tag{A10}$$

The solutions with respect to the initial conditions (A6) read

$$x(t) = v_s\left(t - \frac{1}{\omega}\sin\omega t\right), \quad y(t) = \frac{v_s}{\omega}\left(1 - \cos\omega t\right). \tag{A11}$$

Thus, in this case the trajectory of the vortex core is represented by part of a cycloid. The components of the vortex core velocity are the following:

$$\dot{x}(t) = v_s(1 - \cos\omega t), \qquad \dot{y}(t) = v_s \sin\omega t. \tag{A12}$$

Therefore, using (A8) and (A9) the magnitude of the core velocity is given by

$$v(t) = 2v_s \sin\left(\frac{\omega t}{2}\right) = \frac{2R\chi}{\mu_0 M_{\mathrm{s}}}\frac{B_{\max}}{t_{\mathrm{rise}}}\sin\left(\frac{\omega t}{2}\right). \tag{A13}$$

It can be seen that the point of the trajectory, where the vortex core moves at the fastest speed, is at the apex of the cycloid with a velocity of

$$v_{\max} = 2v_s = \frac{2R\chi}{\mu_0 M_{\mathrm{s}}}\frac{B_{\max}}{t_{\mathrm{rise}}}. \tag{A14}$$

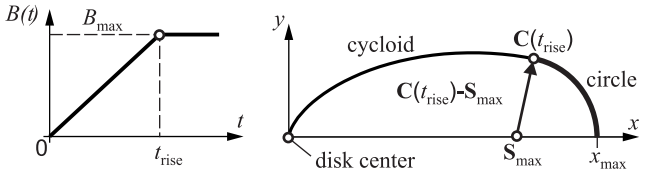

FIG. 9: Left: Assumed shape of a magnetic-field pulse consisting of a linear increase up to $B_{\max}$ during a time interval $\langle 0, t_{\rm rise}\rangle$ and a constant pulse amplitude $B_{\max}$ at instants $t > t_{\rm rise}$. Right: Corresponding vortex core trajectory: part of a cycloid during the interval $\langle 0, t_{\rm rise}\rangle$; a circle at instants $t > t_{\rm rise}$. The core reaches the maximum distance $x_{\max} = s_{\max} + |\mathbf{C}(t_{\rm rise}) - \mathbf{S}_{\max}|$ from the disk center at the point where the trajectory crosses the x axis.

At instants $t > t_{\rm rise}$ we consider the external magnetic field constant and equal to the pulse amplitude $B_{\max}$. Thus, the vortex core continues to move on a circle with a center $\mathbf{S}_{\max} = (s_{\max}, 0, 0)$ and a radius $|\mathbf{C}(t_{\rm rise}) - \mathbf{S}_{\max}|$, see Fig. 9. Hereafter, the core velocity has a constant magnitude

$$v(t_{\rm rise}) = \frac{2 s_{\max}}{t_{\rm rise}} \sin\left(\frac{\omega t_{\rm rise}}{2}\right). \tag{A15}$$

The maximum distance of the core from the disk is located at the x axis, see Fig. 9, and reads

$$\begin{aligned} x_{\max} &= s_{\max} + |\mathbf{C}(t_{\rm rise}) - \mathbf{S}_{\max}| \\ &= s_{\max} + \frac{2 s_{\max}}{\omega t_{\rm rise}} \sin\left(\frac{\omega t_{\rm rise}}{2}\right). \end{aligned} \tag{A16}$$

2. Conditions for dynamic annihilation

In this paragraph we show how the rise time and amplitude of the magnetic-field pulse influences the vortex-core trajectory. The goal is to find appropriate pulse parameters for annihilation of the vortex (the instant when the core leaves the disk area). Therefore, the first condition for annihilation comes from geometry: the core moving on its trajectory has to reach some minimum distance from the disk center. According to our experimental data the minimum distance $R_{\rm an}$, called the annihilation radius R_{an} is about 15% smaller than the disk radius R. Therefore, the first condition has the general form

$$x_{\max} \geq R_{\rm an}. \tag{A17}$$

To avoid vortex polarity switching during the core motion, a second condition must also be fulfilled: the maximum of the core velocity $v_{\max}$ must not exceed the critical core velocity $v_{\rm crit}$, i.e.

$$v_{\max} < v_{\rm crit}. \tag{A18}$$

In the following we focus on discussion at which circumstances both conditions are fulfilled.

a. *Simple dynamic annihilation:* $t_{\rm rise} \to 0$

In this case the vortex-core trajectory is circular almost from the beginning. Annihilation of the vortex requires the displacement $x_{\max}$ of the core equal or greater than the annihilation radius $R_{\rm an}$. Therefore, using the limit case of (A16) the first condition (A17) reads

$$\begin{aligned} x_{\max} &= \lim_{t_{\rm rise}\to 0} \left\{ \frac{R\chi B_{\max}}{\mu_0 M_{\rm s}} \left[1 + \frac{2}{\omega t_{\rm rise}} \sin\left(\frac{\omega t_{\rm rise}}{2}\right)\right]\right\} \\ &= \frac{2 R\chi B_{\max}}{\mu_0 M_{\rm s}} \geq R_{\rm an}. \end{aligned} \tag{A19}$$

Using the limit case of (A15) the second condition (A18) is

$$\begin{aligned} v_{\max} &= \lim_{t_{\rm rise}\to 0} \left[\frac{2R\chi}{\mu_0 M_{\rm s}} \frac{B_{\max}}{t_{\rm rise}} \sin\left(\frac{\omega t_{\rm rise}}{2}\right)\right] \\ &= \frac{\omega R\chi B_{\max}}{\mu_0 M_{\rm s}} < v_{\rm crit}. \end{aligned} \tag{A20}$$

b. *Approaching the static limit:* $t_{\rm rise} \to 2\pi/\omega$

The pulse amplitude required in this case approaches the value of the static annihilation field and the vortex-core trajectory completes one arc of the cycloid. The radius of the following circle trajectory tends to zero, i.e. the core stays in the vicinity of the point $\mathbf{S}_{\max}$. Using (A16) the first condition (A17) determines

$$x_{\max} = \frac{R\chi B_{\max}}{\mu_0 M_{\rm s}} \geq R_{\rm an}. \tag{A21}$$

The magnitude of the core velocity changes according to (A13). Therefore, using (A14) the second condition (A17) reads

$$v_{\max} = \frac{2\omega R\chi B_{\max}}{\pi \mu_0 M_{\rm s}} < v_{\rm crit}. \tag{A22}$$

c. *Short rise time:* $t_{\rm rise} \in (0, \pi/\omega\rangle$

The maximum amplitude $B_{\max}$ is reached before $t = \pi/\omega$, i.e. the vortex core switches from the cycloidal to circular trajectory before it gets to the apex of the cycloid. Using (A16) the first condition (A17) has the following form:

$$x_{\max} = \frac{R\chi B_{\max}}{\mu_0 M_{\rm s}} \left[1 + \frac{2}{\omega t_{\rm rise}} \sin\left(\frac{\omega t_{\rm rise}}{2}\right)\right] \geq R_{\rm an}. \tag{A23}$$

Using (A9) and (A15) the second condition (A18) is given by

$$v_{\max} = \frac{2R\chi}{\mu_0 M_{\rm s}} \frac{B_{\max}}{t_{\rm rise}} \sin\left(\frac{\omega t_{\rm rise}}{2}\right) < v_{\rm crit}. \tag{A24}$$

d. Long rise time: $t_{\mathrm{rise}} \in (\pi/\omega, 2\pi/\omega)$

The maximum amplitude B_{max} is reached after $t = \pi/\omega$, i.e. the vortex core switches from the cycloidal to circular trajectory having passed the apex of the cycloid. Using (A16) the first condition (A17) has the same form as in the previous case:

$$x_{\mathrm{max}} = \frac{R\chi B_{\mathrm{max}}}{\mu_0 M_{\mathrm{s}}}\left[1 + \frac{2}{\omega t_{\mathrm{rise}}}\sin\left(\frac{\omega t_{\mathrm{rise}}}{2}\right)\right] \geq R_{\mathrm{an}}. \tag{A25}$$

However, as the core velocity reaches its maximum at $t = \pi/\omega$ the maximum core velocity changes to the value according to (A14). Therefore, the second condition (A18) determines

$$v_{\mathrm{max}} = \frac{2R\chi}{\mu_0 M_{\mathrm{s}}}\frac{B_{\mathrm{max}}}{t_{\mathrm{rise}}} < v_{\mathrm{crit}}. \tag{A26}$$

3. Phase diagram

Pairs of corresponding values of B_{max} and t_{rise} fulfilling both inequalities, i.e. $x_{\mathrm{max}}(B_{\mathrm{max}}, t_{\mathrm{rise}}) \geq R_{\mathrm{an}}$ and $v_{\mathrm{max}}(B_{\mathrm{max}}, t_{\mathrm{rise}}) < v_{\mathrm{crit}}$, define the pulse parameters needed for successful vortex annihilation. They are displayed as the region of successful core annihilation in Figs. 2, 4, and 5. Note, that $v_{\mathrm{max}}(B_{\mathrm{max}}, t_{\mathrm{rise}})$ is given by (A24) when $t_{\mathrm{rise}} < \pi/\omega$ and by (A26) when $t_{\mathrm{rise}} > \pi/\omega$.

Appendix B: Dynamics in the core-flipping regime

In case of high pulse amplitudes and/or short rise times the core velocity exceeds the critical velocity, the core polarity is switched and the sense of the vortex core gyration is reversed. This significantly reduces the efficiency of the magnetic field pulse on the vortex core displacement (the maximum amplitude of the vortex core gyration). Fig. 10 shows how changes in the pulse amplitude and rise time affect the maximum core displacement from the disk center in the core-flipping regime [region (3) of the pulse rise time – pulse amplitude phase diagram]. The pulse amplitude is higher than the threshold dynamic annihilation field for all three pulses. Increasing a pulse amplitude from -8.5 mT to -10.8 mT while keeping the rise time constant leads to an increase in the maximum displacement of about 100 nm. However, a further increase of the amplitude to -11.4 mT and shortening the rise time to 2.5 ns at the same time leads to an overall decrease in the maximum displacement to the value induced by the first pulse.

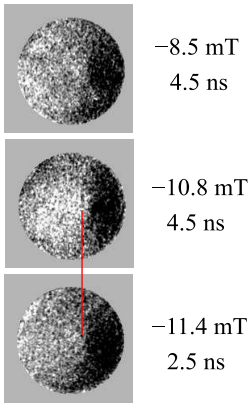

FIG. 10: Demonstration of the reduced effectivity of the magnetic field pulse on the maximum displacement of the vortex core in the core-flipping regime. The disk is 2500 nm wide and 20 nm thick. Each image is a snapshot of the maximum core displacement during a particular pulse. Increasing the amplitude leads to a progressive increase in the maximum displacement (the black domain shrinking due to a negative pulse). However, a decrease of the rise time of the pulse with the highest amplitude leads to an overall decrease of the maximum displacement of about 100 nm despite the increased amplitude. The red line is a guide to the eye.

* Electronic address: urbanek@fme.vutbr.cz
† Electronic address: vojtech.uhlir@uh.cz

[1] A. Hubert and R. Schäfer, *Magnetic Domains - The Analysis of Magnetic Microstructures* (Springer, Berlin, 1998), ISBN 3-540-64108-4.
[2] T. Shinjo, T. Okuno, R. Hassdorf, K. Shigeto, and T. Ono, Science **289**, 930 (2000).
[3] A. Wachowiak, J. Wiebe, M. Bode, O. Pietzsch, M. Morgenstern, and R. Wiesendanger, Science **298**, 298 (2002).
[4] K. Y. Guslienko, J. Nanosci. Nanotechnol. **8**, 2745 (2008).
[5] M.-Y. Im, P. Fischer, K. Yamada, T. Sato, S. Kasai, Y. Nakatani, and T. Ono, Nat. Commun. **3**, 983 (2012).
[6] S. Bohlens, B. Kruger, A. Drews, M. Bolte, G. Meier, and D. Pfannkuche, Appl. Phys. Lett. **93**, 142508 (2008).
[7] S.-K. Kim, K.-S. Lee, Y.-S. Yu, and Y.-S. Choi, Appl. Phys. Lett. **92**, 022509 (2008).
[8] N. Kikuchi, S. Okamoto, O. Kitakami, Y. Shimada, S. G. Kim, Y. Otani, and K. Fukamichi, J. Appl. Phys. **90**, 6548 (2001).
[9] M. Schneider, H. Hoffmann, and J. Zweck, Appl. Phys. Lett. **79**, 3113 (2001).
[10] B. Van Waeyenberge, A. Puzic, H. Stoll, K. W. Chou, T. Tyliszczak, R. Hertel, M. Fähnle, H. Brückl, K. Rott, G. Reiss, et al., Nature **444**, 461 (2006).
[11] V. Uhlíř, M. Urbánek, L. Hladík, J. Spousta, M.-Y. Im, P. Fischer, N. Eibagi, J. J. Kan, E. E. Fullerton, and T. Šikola, Nat. Nanotechnol. **8**, 341 (2013).
[12] A. A. Thiele, Phys. Rev. Lett. **30**, 230 (1973).
[13] D. L. Huber, Phys. Rev. B **26**, 3758 (1982).
[14] V. Novosad, F. Y. Fradin, P. E. Roy, K. Buchanan, K. Y.

Guslienko, and S. D. Bader, Phys. Rev. B **72**, 024455 (2005).
[15] K. S. Buchanan, P. E. Roy, F. Y. Fradin, K. Y. Guslienko, M. Grimsditch, S. D. Bader, and V. Novosad, J. Appl. Phys. **99**, 08C707 (2006).
[16] K.-S. Lee and S.-K. Kim, Appl. Phys. Lett. **91**, 132511 (2007).
[17] K. Y. Guslienko, R. H. Heredero, and O. Chubykalo-Fesenko, Phys. Rev. B **82**, 014402 (2010).
[18] O. V. Sukhostavets, B. Pigeau, S. Sangiao, G. de Loubens, V. V. Naletov, O. Klein, K. Mitsuzuka, S. Andrieu, F. Montaigne, and K. Y. Guslienko, Phys. Rev. Lett. **111**, 247601 (2013).
[19] B. Pigeau, G. de Loubens, O. Klein, A. Riegler, F. Lochner, G. Schmidt, and L. W. Molenkamp, Nature Phys. **7**, 26 (2011).
[20] R. L. Compton, T. Y. Chen, and P. A. Crowell, Phys. Rev. B **81**, 144412 (2010).
[21] T. Y. Chen, M. J. Erickson, P. A. Crowell, and C. Leighton, Phys. Rev. Lett. **109**, 097202 (2012).
[22] P. Fischer, Mater. Today **13**, 14 (2010).
[23] S. Kasai, P. Fischer, M.-Y. Im, K. Yamada, Y. Nakatani, K. Kobayashi, H. Kohno, and T. Ono, Phys. Rev. Lett. **101**, 237203 (2008).
[24] S.-B. Choe, Y. Acremann, A. Scholl, A. Bauer, A. Doran, J. Stöhr, and H. A. Padmore, Science **304**, 420 (2004).
[25] K. Y. Guslienko, B. A. Ivanov, V. Novosad, Y. Otani, H. Shima, and K. Fukamichi, J. Appl. Phys. **91**, 8037 (2002).
[26] K. Y. Guslienko, V. Novosad, Y. Otani, H. Shima, and K. Fukamichi, Appl. Phys. Lett. **78**, 3848 (2001).
[27] K. Y. Guslienko, K.-S. Lee, and S.-K. Kim, Phys. Rev. Lett. **100**, 027203 (2008).
[28] K.-S. Lee, S.-K. Kim, Y.-S. Yu, Y.-S. Choi, K. Y. Guslienko, H. Jung, and P. Fischer, Phys. Rev. Lett. **101**, 267206 (2008).
[29] K. S. Buchanan, P. E. Roy, M. Grimsditch, F. Y. Fradin, K. Y. Guslienko, S. D. Bader, and V. Novosad, Phys. Rev. B **74**, 064404 (2006).
[30] X. M. Cheng, K. S. Buchanan, R. Divan, K. Y. Guslienko, and D. J. Keavney, Phys. Rev. B **79**, 172411 (2009).
[31] T. Uhlig, M. Rahm, C. Dietrich, R. Höllinger, M. Heumann, D. Weiss, and J. Zweck, Phys. Rev. Lett. **95**, 237205 (2005).
[32] T. Y. Chen, A. T. Galkiewicz, and P. A. Crowell, Phys. Rev. B **85**, 180406 (2012).
[33] P. Wessels, J. Ewald, M. Wieland, T. Nisius, A. Vogel, J. Viefhaus, G. Meier, T. Wilhein, and M. Drescher, Physical Review B **90**, 184417 (2014).
[34] M. J. Donahue and D. G. Porter, *OOMMF users guide, version 1.0, interagency report NISTIR 6376* (National Institute of Standards and Technology, Gaithersburg, MD, 1999).
[35] Pulses with an amplitude approaching or exceeding $B_{\mathrm{an-stat}}$ and a sufficient duration will annihilate the vortex no matter what the exact dynamic behavior is. During preparation of the manuscript we became aware of the work[33] which demonstrates the annihilation of the vortex core in 2×2-$\mu\mathrm{m}^2$, 30-nm-thick permalloy squares by a high amplitude ($\sim 4 \times B_{\mathrm{an-stat}}$), sub-nanosecond gaussian pulse.
[36] The values of v_{crit} estimated from fitting the boundaries of the phase diagram to our experimental data were $323 \pm 15\,\mathrm{m\,s^{-1}}$ and $307 \pm 10\,\mathrm{m\,s^{-1}}$ for the 1600-nm-wide, 20-nm-thick disk and the 1600-nm-wide, 30-nm-thick disk, respectively [see Figs. 2(a, b)].
[37] The micromagnetic simulations were carried out using OOMMF[34]. The nanodisks were discretized into cubes with dimensions of $4 \times 4 \times 4\,\mathrm{nm}^3$. Zero magnetocrystalline anisotropy and an exchange constant of $A_{\mathrm{ex}} = 10\,\mathrm{pJ\,m^{-1}}$ (typical for permalloy) were used. The spontaneous magnetization $\mathrm{M_s}$, gyromagnetic ratio γ and damping parameter α were determined experimentally using ferromagnetic resonance on blanket film samples, with values: $M_{\mathrm{s}} = 690\,\mathrm{kA/m}$, $\gamma = 2.09 \times 10^{11}\,\mathrm{rad{\cdot}Hz/T}$ and $\alpha = 0.0072$. The M_{s} value was verified by vibrating sample magnetometry.